Accuracy Assessment of 3D model generation using High Resolution Stereo-Optical Satellite Imagery

MAHMOUD S. MAHMOUD[a], ELHADI K. MUSTAFA[b], AMR H.AHMED ALI[a], HOSAM E. ELSSEMARY[a]

[a]Benha University, Faculty of Engineering-Shoubra, Surveying Engineering Department
[b]Khartoum University, Faculty of Engineering, Surveying Engineering Department

ABSTRACT

Three dimensional model generations represents a continuous area of research, where there was a great demand for it in day to day applications. These applications move from electromagnetic propagation for telecommunication to more demanding simulations for acoustic, urban planning, virtual and augmented reality. Year after year radiometric quality and geometric accuracy of new high resolution satellites keep on improving so much where satellite imagery become a real potential solution for the production of such digital elevation models. This paper evaluates the accuracy of High Resolution Stereo-Optical Satellite Imagery (HRSI) for digital surface model production using Leica Photogrammetry Suite (LPS). A well distributed set of ground control points was determined and then surveyed using GPS technique. These points were then divided into two sets: one will act as control set; while the other will be the check points set in order to evaluate the accuracy of the 3D model and the extracted digital elevation model. These control points allow for qualitative and quantitative evaluation process. Several experiments have been performed to evaluate the 3D model from Stereo-Optical Satellite Imagery. The result of RMSe of the experiments with 3 control points showed a horizontal absolute accuracy of 0.61 m for East direction and 0.68 m for north direction. Meanwhile, the vertical absolute accuracy reaches 1.05 m. However, the best accuracy achieved using 10 control points to be 0.58 min east direction and 0.67 m in north direction for the representation of the horizontal absolute accuracy and 0.81 m for the vertical absolute accuracy. Finally, conclusions and recommendations for further research have been highlighted.

KEYWORDS: Stereo-Optical Satellite Imagery**,** Orthorectification, Digital Elevation Model, Horizontal Accuracy, Vertical Accuracy.

1. INTRODUCTION

Topography is the base for many earth's surface processes and thus finds applications in many fields such as hydrology, security, military, agriculture, climatology, communication, mining works, roads route (selection, design and execution) and other disciplines. Topographic mapping plays a tremendous role in local, national and international basis. Due to this fact, topographic mapping received good attention all over the world. The importance of topographic mapping as a national project is therefore growing rapidly. Also, the coin of geographic information system software, topographic maps and digital elevation models become the essential component of national geospatial data infrastructure. In developed countries, revised and up-to-date

maps are continuously produced using current elevation data captured by remote sensing sensors. In developing countries, governmental Mapping Corporation and private mapping firms are lagging far away to produce fresh topographic maps or even to revise the existing ones at regular time intervals. This dim status is due to the fact of shortage, inadequate technical capacities in the area of geo-information and lack of knowledge about the importance and role of topographic maps and digital elevation models (DEMs) in local and national development. Taking Sudan as an example, only 200 topographic map (1:100,000) sheets out of 920 for the full coverage have been produced, covering only selected areas (Gar Alnabi et al., 2011a). In addition, and up to now, no endeavors have been made by any Sudanese mapping corporation or firm to generate digital elevation models. Unfortunately, the process of extracting topographical information from existing topographical maps and integrating them in a new digital topographical map is usually a lengthy and time consuming process due to differences in map units and contour intervals (Gar Alnabi et al., 2011b).Currently, there are many satellites that offer stereo satellite imagery, such asCarto-sat1, CHRIS/PROBA, EROS-A, IRS, IKONOS, MOMS-02, and SPOT.

The studies of the application of IKONOS and SPOT5 imagery for mapping were already published. They showed that high-resolution satellite imagery was effective for mapping (Iida et al., 2001). The 3D accuracy and bias compensation of IKONOS imagery were already studied (Fraser et al., 2002). Substantial research work has been conducted using stereo satellite imagery to map the Earth's surface. Different procedures are used to extract the information, such as digital elevation models (DEMs) and orthoimages using imagery from SPOT satellites (Chen and Lee, 1993). Nevertheless, the highest scale of mapping that can be achieved is scale. 1:50,000 due to the coarse spatial resolution of the SPOT satellite image (20 m). Currently, the existence of the high spatial resolutions of less than a meter could serve numerous applications such as Earth monitoring, environmental modeling, geometric measurement and creation of the digital elevation models.

The main objective of this study is to analyze and evaluate the DEM generated from High Resolution Stereo-Optical Satellite Imagery, and absolute differences between the generated DEM and User-defined 3D coordinates by means of GPS observation.

2. DIGITAL ELEVATION MODEL

DEM consists of a pattern of data points of known horizontal coordinates (x, y) and height (z) which representing the terrain surface.DEM can be created from different pattern of data points depending on the collection procedures and used techniques. Data for DEM can be created by (ASPRS, 2001):

- Digitizing the contour maps.
- Direct field observation by land surveying specially the GPS or Total Station.
- Analytical or digital photograrnrnetric procedures.

The recent available technology to produce DEM automatically without assistance of ground control points are: i) The inventory systems that integrate high accuracy inertial measurement unit (IMU) with a global positioning system (GPS) and a computer on

board mapping aircraft; ii) from digital surface model. Unfortunately, these methods are either time consuming (each sampling point has to be measured individually) and/or require experts, and a set of detailed control points. As an alternative, DEM could be produced with small scales using satellite base imaging such as SPOT and IKONOS (Lerome et al., 2009). DEM creation implies the sequence of six processing steps. This routine is used for the creation of a DEM based on stereo images. These Steps are summarized as (Toutin, 2001):

- Acquisition and pre-processing of remotely sensed data (images and metadata) to determine an approximate value for each parameter of 3D physical model.
- Collection of ground control points (GCPs).
- Computation of the 3 D stereo model
- Image matching.
- Computation of X, Y and Z cartographic coordinates from determined corresponding image coordinates
- Creation of regular grid spacing with interpolation or mismatched areas and eliminating points not belonging.

The root-mean-square error (RMSe) is used as a measure of how closely a data set matches the actual world DEM which is considered to be the reference model should have a higher accuracy (Zhen et al., 2001). In the case of DEMs acquired by means of space images, the accuracy is mostly depending upon the image resolution (ground pixel size), base-to-height ratio and image contrast (radiometric quality). A difference between a relative and an absolute accuracy can be noticed when systematic image errors have not be respected and the orientation quality is limited (WANG et al., 2008). The standard deviation (SZ) can be used as well for describing the accuracy of a DEM. The vertical accuracy (the accuracy of a height) is depending upon the accuracy of the x-parallax (Spx) and the base to-height ratio of the imaging configuration “h/b“(Poli et al., 2004).

$$SZ = Scale * \frac{h}{b} * Spx \quad (1)$$

$$SZ = Pixel\ Size * a * \frac{h}{b} \quad (2)$$

Equations (1) and (2) are used for computing the standard deviation in the case of digital space images. The value of the parameter"a"which is a multiplication factor is usually below one pixel and the accuracy of the x-parallax (Spx) is depending upon the contrast and is also usually below one pixel.

3. THE STEREO HRSI CONCEPT

Stereo products consist of two satellite images of the same location on Earth, taken from two different perspectives during one orbital pass. The pair of images is collected in-track, or on the same ground path just moments apart to maintain the tonal consistency between each image, enabling better interpretability. In our case, IKONOS stereo pair contains an image collected at a low elevation angle (above 60 degrees) as well as an image collected at a higher elevation angle (above 72 degrees) with 30°-45° convergence (0.54 to 0.83 base-to-height ratio).

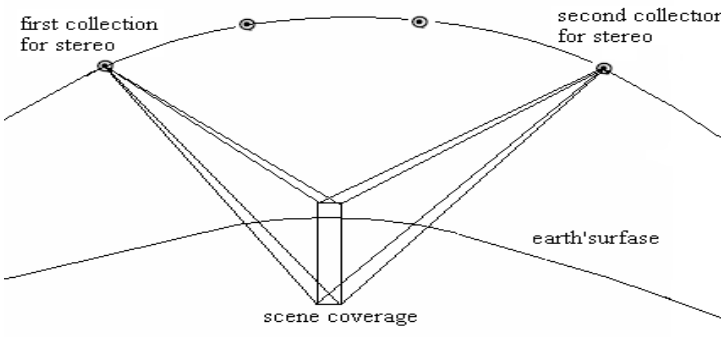

Figure (1): Stereo IKONOS Satellite Image data collection

Reference Stereo products have a horizontal accuracy of 25 meters CE90 (Circular Error 90%) and a vertical accuracy of 22 meters LE90 (Linear Error of 90%) without any Ground Control Points (GCPs). When reliable GPS derived GCP is available the horizontal and vertical Geospatial accuracies increase to <2.5m horizontal and <1.5m vertical (Satellite Imaging corporation, 2012).

4. MATHEMATICAL MODEL FOR HRSI

Sensor models are of particular importance to stereo reconstruction, image Ortho-rectification and DEM generation, where they are essential to establish the functional relationship between the image space and the object space. Sensor models are typically classified into two categories: physical and generalized models. Recently, generalized models has gained considerable interest due to the requirement of real time processing and that the photogrammetric processing can be kept unchanged when deal with different sensors data as these generalized sensor models are independent. Therefore, the generalized sensor models are more common to be used in mapping community (Tao et al., 2000).

For IKONOS stereo images, the sensor physical parameters are derived from the satellite ephemeris and attitude data without using ground control points. The satellite ephemeris data are determined using on-board GPS receivers and sophisticated ground processing of the GPS data. The satellite altitude is determined by optimally combining star tracker data with measurements taken by the on-board gyros. Since the IKONOS satellite imagery vendor, Space Imaging Company, has not released the satellite ephemeris data, no physical mathematical model can be established. Consequently, some generalized generic mathematical models are needed to substitute the physical models for IKONOS Imagery restitution (Hu et al., 2004).However, the most common applied mathematical model is the rational function model (RFM) (Tao and Hu, 2001).

The Rational Function Model is a generalized model that is widely used. During the few past years, RFM has come into widespread use within the intelligence community. This imaging geometry model uses ratios of two 3D order polynomial functions to compute the image coordinates (McGlone, 1996). The IKONOS satellite image company, Space Imaging, calculates the rational polynomial coefficients (RPCs) for each Image and distributes these data with the images. Since rational polynomial

considers heights into geometric correction, it is more adequate than 2D polynomials. It can be considered as the best choice when there is no information about the image and then a rigorous modeling cannot be used (as in the case of IKONOS satellite imageries).The validation of (RFM) model has been tested in several researches with aerial photography data and satellite imageries (Tao et al., 2000). The RFM can be represented as follows:

$$x = \frac{P1(X,Y,Z)}{P2(X,Y,Z)} = \frac{\sum_{i=0}^{m1}\sum_{j=0}^{m2}\sum_{k=0}^{m3} a_{ijk}X^iY^iZ^i}{\sum_{i=0}^{n1}\sum_{j=0}^{n2}\sum_{k=0}^{n3} b_{ijk}X^iY^iZ^i} \quad (3)$$

$$y = \frac{P1(X,Y,Z)}{P2(X,Y,Z)} = \frac{\sum_{i=0}^{m1}\sum_{j=0}^{m2}\sum_{k=0}^{m3} c_{ijk}X^iY^iZ^i}{\sum_{i=0}^{n1}\sum_{j=0}^{n2}\sum_{k=0}^{n3} d_{ijk}X^iY^iZ^i} \quad (4)$$

Where,

x,y	Image coordinates
X,Y,Z	Ground coordinates
a_{ijk}, b_{ijk},c_{ijk},d_{ijk}	Polynomial coefficient (total 80)
m_1,m_2,m_3,n_1,n_2,n_3	0-3 , where $i+j+k \leq 3$

The RPCs are calculated by Space Imaging from the satellite ephemeris and attitude data instead of releasing the ephemeris data themselves. Therefore, the RFM model is implemented by most of the commercial software packages in order to use the supplied RPCs. This software modules deal with IKONOS satellite images by reading the RPC files and applying the RFM model to orient the IKONOS imageries (ELASHMAWY, 2005).

5. STUDY AREA AND STEREO IKONOS IMAGES ACQUISITION

The test area (Wadi seidna) is located at the north of Khartoum in Sudan bout 16km north of Omdurman city and geographically, it lies between Upper left corner coordinates of (444535.977, 1747921.762) and Lower right corner coordinates of (449800.083, 1742045.500). The elevation range of this area is about 60 m. The study area is about 31 Square Kilometers. Figures (2) and (3) show the general location of the study area.

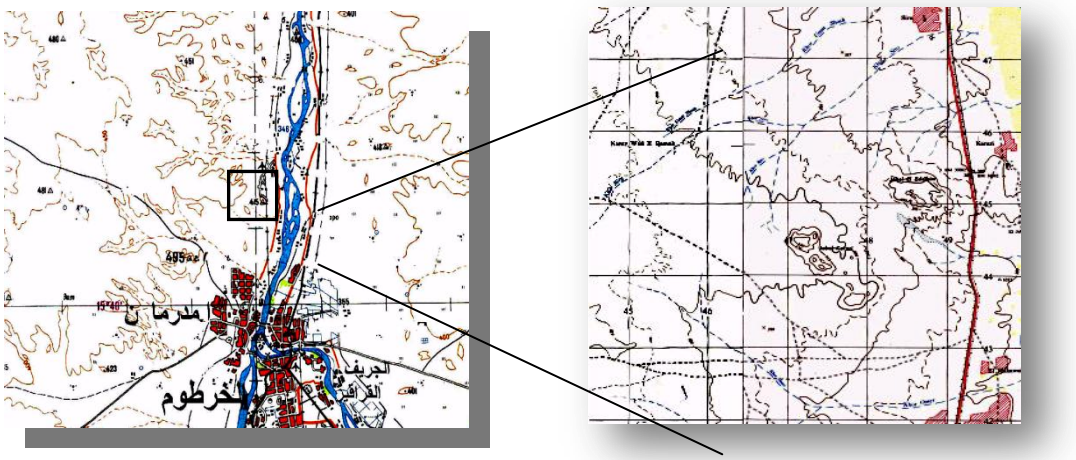

Figure (2): general location of the study area

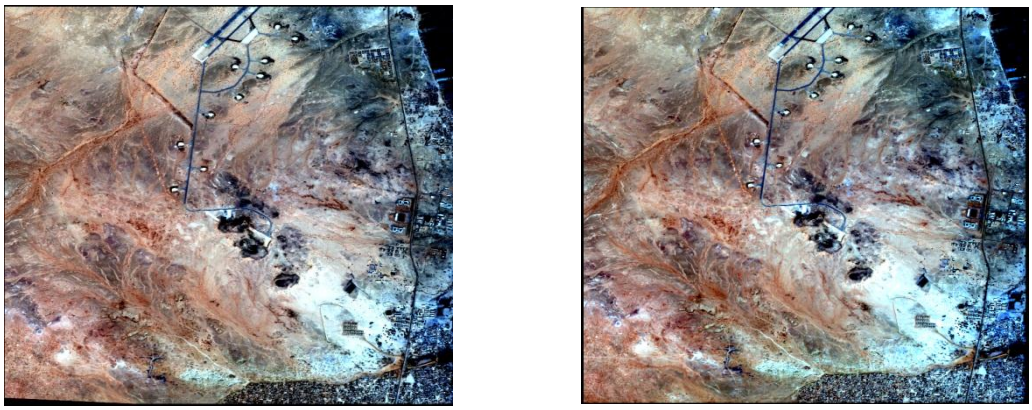

(a) Left Image (b) Right Image

Figure (3): IKONOS HRS 1M stereo-pair of the study area

Stereo IKONOS satellite images, with 1m resolution, covering the study area were acquired over SUDAN. These data are delivered in Geo-Tiff format with text files containing the Rational Polynomial Coefficients (RPC) for each image. These RPCs are important for rectifying IKONOS satellite images using Rational Function Model instead of the rigorous models that require the ephemeris data of the satellite orbit. Table (1) shows the Main parameters of the available IKONOS HRS 1M stereo-pair

Table (1): Main parameters of the available IKONOS HRS 1M stereo-pair

Acquisition Date/Time	08:41 GMT 27-12-2003 and 08:42 GMT 27-12-2003
Sun Angle Azimuth	156.1241 and156.3809 degrees
Sun Angle Elevation	63.50707 and 47.50945 degrees
Overlap	99%
Rows	5893 and 6004 pixels
Columns	5351 and 5357 pixels
Pixel Size X	1.000 meters
Pixel Size Y	1.000 meters
Percent Component Cloud Cover	0
Size (km)	5.808 km * 5.344 km
Area	31 Square Kilometers

6. RESEARCH METHODOLOGY

The framework model of the methodology used in generating the DEM from stereo pair satellite images is shown in Figure (4).

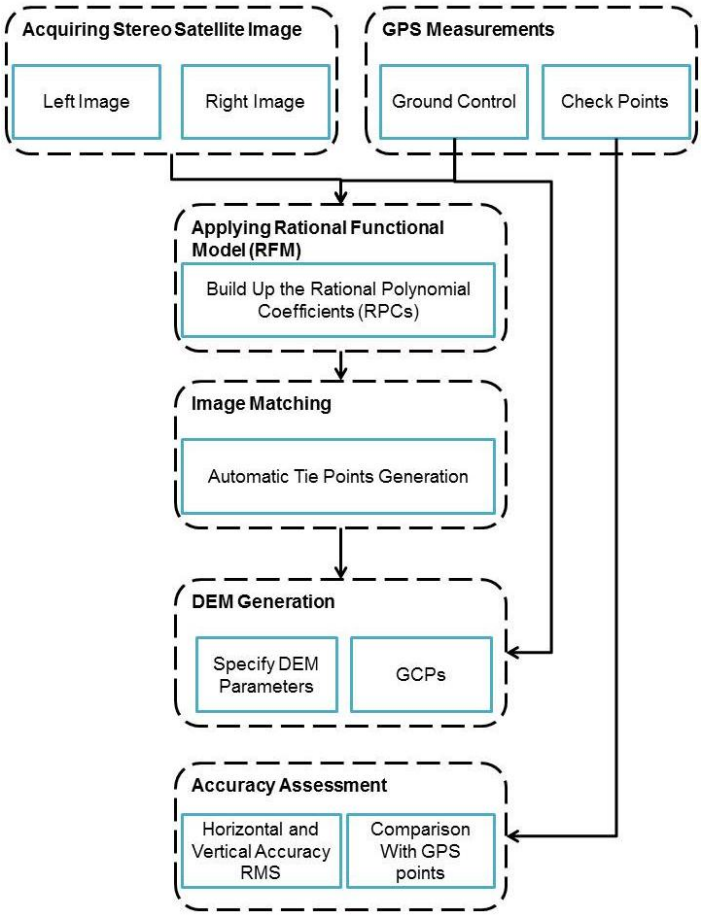

Figure (4): Conceptual framework model of the methodology used for extracting the DEM

The next subsections will explain each of the previous steps.

6.1. Acquiring Stereo IKONOS Satellite imagery

Initially, selecting the stereo-pair images is a fundamental step for both matching the coverage area and the accuracy. The key selection criteria of the stereo-pair images are:

a. Base Height Ratio (B/H): The B/H ratio between the observation base B (distance between two satellite positions) and the height H (satellite elevation)
b. Time Lag: it is important that the time lag between the two images to be as short as possible to avoid any excessive radiometric differences that reduce the accuracy.
c. Degree of Overlap: Normally, the common part between the two stereo-pairs depends particularly on the difference in orientation of the two images and always evaluated by the geographic coordinates of the two scenes.
d. The pixel size of the image should be chosen according to the original map scale in order to preserve the planimetric accuracy of the map (i.e. 0.2mmat the map scale) (Thomas, 2002).

$$\text{Pixel size} = 0.2\text{mm} * \text{Map Scale} \quad (5)$$

6.2. Building the Rational Polynomial Coefficients (RPCs)

The generation of a DEM from stereo-pair images requires rational polynomial coefficients (RPCs) positioning from the satellite sensor. These RPCs would be used to generate the tie points and calculate the stereo-pair images relationship. The IKONOS sensor model supports IKONOS imagery and its associated rational polynomial coefficient (RPC) and metadata files. The metadata files contain information regarding the images in the data set. RPC files contain the necessary information to determine interior and exterior orientation.

6.3. Defining the Ground control Points

Collection of ground control and check points are needed. One of the fastest and accurate techniques is the Global Positioning System (GPS). Before selecting the point locations on the ground, the best well-identified points on the images were selected such that they are well distributed all over the common area of the stereo images. These locations are easily identifiable; mostly corners of buildings, and some road intersections.

Static differential GPS technique was used for measuring the ground control Points, the most accurate technique. Two well identified points of the High Accuracy Reference Network provided by the Sudanese Survey Authority, near the study area, were chosen as reference stations. Ten out of twenty two points were selected to be ground control points and the other twelve points were used as check points. Figure 5 shows the distribution of control and check points. Geo-referencing and stereo-model setup of the images was established using different numbers and different distribution of GCPs (Three, Four, Six, Eight and Ten Ground control points). The 10 red pyramid points represent the Ground Control Points, while the rest of the points (rounded green points are used as check points).

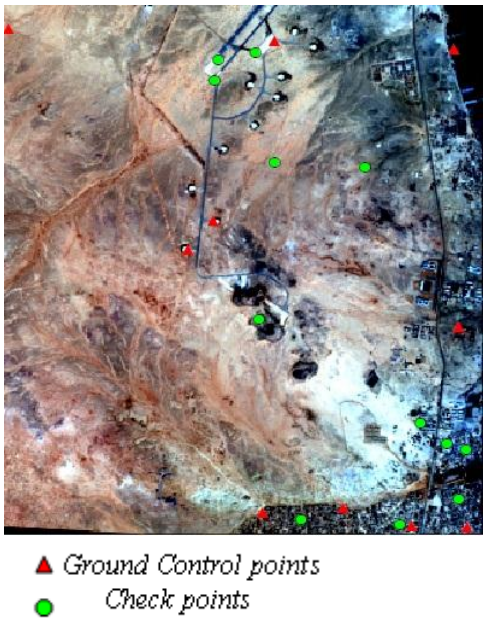

Figure (5): Ground control points and check for IKONOS HRS stereo-pair

6.4. Defining the Tie Points

A tie point is a point whose ground coordinates is not known, but is visually recognizable in the overlap area between two or more images. The corresponding image positions of tie points appearing on the overlap areas of multiple images is identified and measured. Ground coordinates for tie points are computed during block triangulation. Tie points can be measured either manually or automatically. Automatic Tie Point option was used in this research, where 60 tie points were selected along the two scenes as shown in Figure (6).

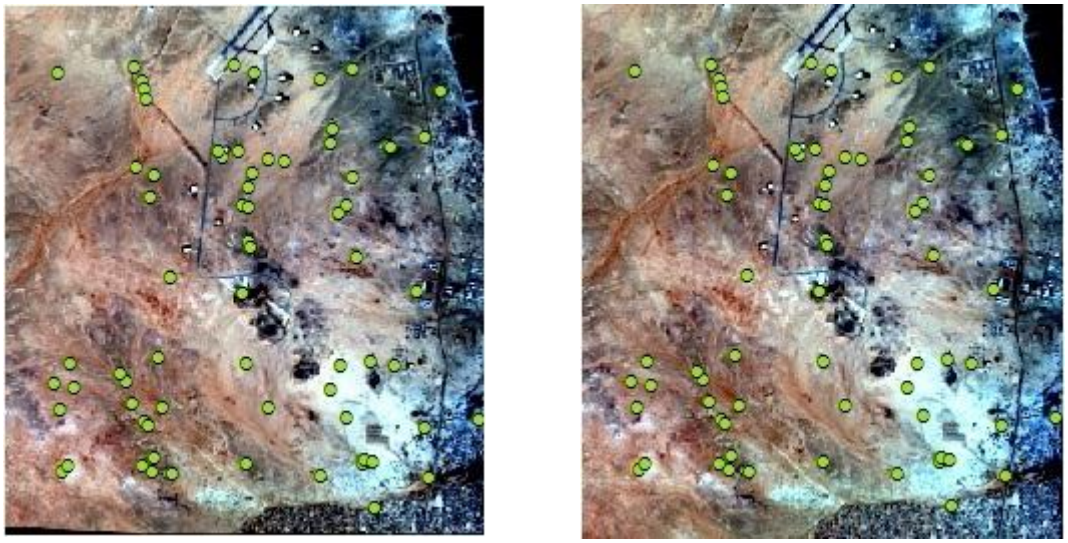

Figure (6): Tie points for IKONOS HRS stereo-pair

6.5. DEM parameters

The DEM with the best accuracy was produced with the parameters shown in table (2):

Table (2): The basic parameters of the output DEM

Output projection	Universal Transverse Mercator Zone 36 North
Datum	WGS84
Units	Meters
Cell size	[3 x 3] meters
Search Size	17 x 3
Correlation Size	7 x7
Coefficient Limit	0.800, the minimal correlation coefficient for a match to be accepted as a correct match. The value can be from 0.10 to 0.99
Topographic Type	Rolling Hills
DTM Filtering	Moderate

6.6. The Output DEM

The DEMs was generated from IKONOS stereo imagery by using the Leica Photogrammetry Suite (LPS), once the six steps are carried out and the parameters of

the output DEM are set up, the final step of extracting the DEM is conducted. Finally, different DTMs can be constructed depending on the specified DTM output type "American Standard Code for Information Interchange (ASCII) files; TerraModel; Triangulated Irregular Networks (TIN); raster DEMs Environmental System Research Institute (ESRI) 3D Shape files". Herein, the final rectified DEM is shown in Figure (7).

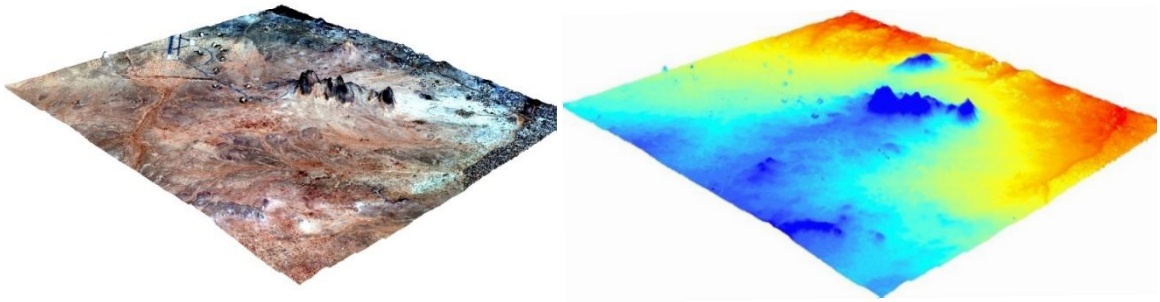

Figure (7): Output of DEM produced fromStereo-HRS data

6.6.1. Evaluation of the produced DEM

It is important to examine the resulted DEM against other data sources to ensure the accuracy and harmony of the simulation model. The following 3D reference sources can be used to calculate DTM accuracy:

- Check points contained within a block file
- Ground Control Points contained within a block file
- Tie points (whose XYZ coordinates have been computed) "contained within a block file"
- External raster DEM
- User-defined 3D coordinates contained within an ASCII file

On the other hand Real Time Kinematic "RTK" GPS can deliver almost instantaneous point coordinates with centimeter-level accuracy. There are many applications that can take advantage of RTK technology, including topographic surveying, engineering construction, geodetic control, vehicle guidance and automation, etc.

In our case, Leica dual frequency GPS receivers were placed on a pole and a 100 M recording interval was selected. A reference receiver was placed near the test field. In all observing sessions the GDOP (Geometric dilution of precision) value varied between 3 to 6 and the SNR (Signal-to-noise ratio) values for almost all satellites were at their maximum. Finally Reduction and analysis of GPS measurements were carried out using the Leica Geo-Office software.

7. RESULTS AND ANALYSES

Several experiments have been accomplished in order to apply the above procedures, the assessment of the accuracy of the produced stereo image and generated DEM have been applied as described in the below sections.

7.1. Evaluation of horizontal and vertical spatial accuracy of the model

In order to assess the model applied for generating the stereo image, the performance of the model is discussed in relation to the numbers of ground control points; under conditions of well-defined and well distributed ground control points. Five experiments have been performed using different number of Ground Control Points "GCPs". Then the horizontal accuracy and vertical accuracy evaluated through 12 Check Points "CP". The number of GCPs per each experiment defined at table (3) and presented at figure (8 a, b, c, d, e)

Table (3): Number of GCP for each case

Experiment	No. of (GCP)
Case one	3
Case two	4
Case three	6
Case four	8
Case five	10

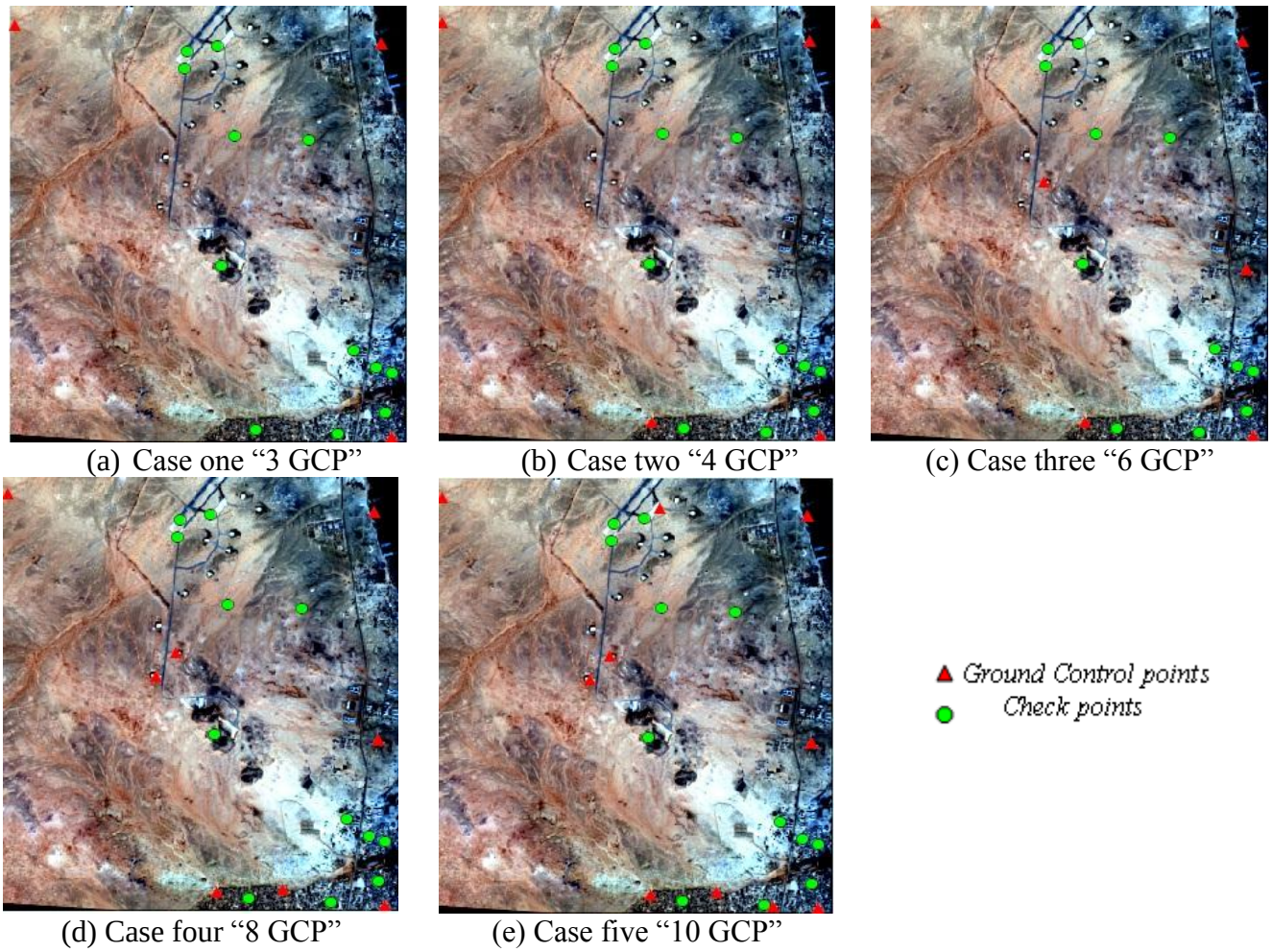

(a) Case one "3 GCP" (b) Case two "4 GCP" (c) Case three "6 GCP"

(d) Case four "8 GCP" (e) Case five "10 GCP"

Figure (8): Different numbers and distributions of GCPs for Geo-referencing and Stereo-model setup of the images

The results of the horizontal shift that defined as the resultant of the X-residuals and Y-residuals for the GCPs and the 12CP per each case of the above mentioned cases are presented at figure (9a, 10a, 11a, 12a, 13a). Also, the results of the height (vertical) shift for the GCPs and the 12 CP are presented at figure (9b, 10b, 11b, 12b, 13b).Furthermore, these results are tabulated at table (4, 5, 6, 7, and 8).

Table (4): Results of Case 1 (3 GCPs and 12 CPs)

Pnt	RX	RY	RZ	Pnt	RX	RY	RZ
GCP 27	0.1084	0.5039	0.1844	**CP 37**	-0.3079	0.8169	0.9793
GCP 28	0.4496	-0.1101	0.3873	**CP 38**	-0.3372	0.0672	2.1896
GCP 29	-0.6437	-0.4346	-0.5716	**CP 39**	-0.0121	0.0164	0.4509
CP 30	0.1953	-1.0199	-0.3166	**CP 41**	-0.2179	0.5995	0.4103
CP 33	-1.1945	-0.5341	0.9464	**CP 47**	-1.2706	-0.0792	1.4893
CP 34	0.1642	-0.6175	0.4103	**CP 32**	-0.7794	0.6806	0.962
CP 35	0.5669	-1.2075	-0.9584	**CP 42**	0.1271	0.4703	0.7344
CP 36	0.3186	-0.8057	1.1774				

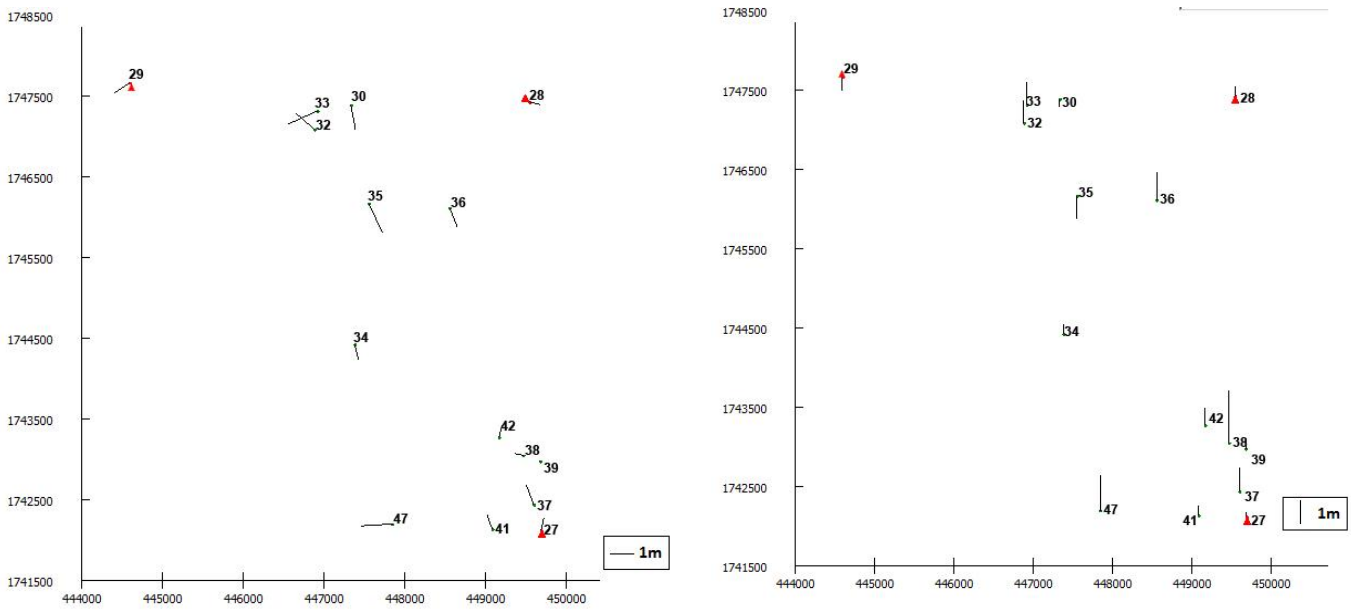

(a) horizontal resultant (b) vertical shift

Figure (9): Horizontal resultant (Right) and vertical shift (Left) for the GCPs and 12 CP of Case 1

From table (4) it can be seen that the absolute shift in east direction ranges from 0.01 m to 1.27 m. Concerning the shift in north direction, the absolute shift ranges from 0.02 m to 1.21 m. The horizontal resultant ranges from 0.02m to 1.33m that illustrated in figure (9a). Figure (9b) illustrates the case of height shift for case 1, where the values range from 0.18m to 2.19m.

Table (5): Results of Case 2 (4 GCPs and 12 CPs)

Pnt	RX	RY	RZ	Pnt	RX	RY	RZ
GCP 27	0.07	0.48	0.18	**CP 37**	-0.35	0.80	0.98
GCP 28	0.41	-0.13	0.39	**CP 38**	-0.38	0.05	2.19
GCP 29	-0.69	-0.46	-0.57	**CP 39**	-0.05	0.004	0.45
GCP 43	-0.01	0.53	0.002	**CP 41**	-0.26	0.58	0.41
CP 33	-1.24	-0.55	0.94	**CP 47**	-1.31	-0.10	1.49
CP 34	0.12	-0.64	0.41	**CP 32**	-0.82	0.66	0.96
CP 35	0.53	-1.23	-0.96	**CP 42**	0.09	0.45	0.73
CP 36	0.28	-0.83	1.18	**CP 30**	0.15	-1.04	-0.32

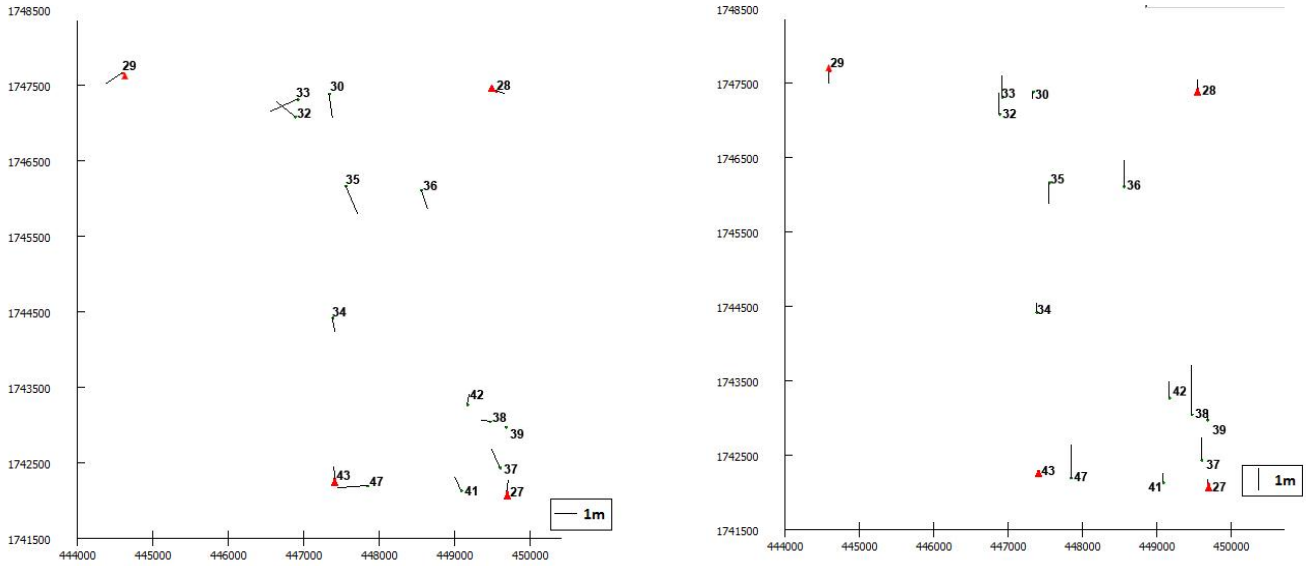

(a) horizontal resultant (b) vertical shift

Figure (10): Horizontal resultant (Right) and vertical shift (Left) for the GCPs and 12 CP of Case 2

In case 2, there was no significant changes, whereas presented at table (5) the absolute shift in east direction ranges from 0.01 m to 1.31 m. on the other hand, the shift in north direction, the absolute shift ranges from 0.004 m to 1.23 m. Consequently, the horizontal resultant ranges from 0.05 m to 1.34 m. The horizontal resultant values are illustrated in figure (10a). Figure (10b) illustrates the case of height shift, where the values range from 0.002m to 2.19 m.

Table (6): Results of Case 3 (6 GCPs and 12 CPs)

Pnt	RX	RY	RZ	Pnt	RX	RY	RZ
GCP 27	-0.02	0.67	0.05	**CP 38**	-0.46	0.23	2.05
GCP 28	0.32	0.05	0.25	**CP 39**	-0.14	0.18	0.31
GCP 29	-0.77	-0.27	-0.71	**CP 41**	-0.35	0.76	0.27
GCP 43	-0.10	0.71	-0.14	**CP 47**	-1.40	0.08	1.35
GCP 44	0.04	-0.45	0.27	**CP 32**	-0.91	0.84	0.82

Pnt	RX	RY	RZ	Pnt	RX	RY	RZ
GCP 45	0.77	-0.78	0.27	**CP 42**	0.00	0.63	0.60
CP 35	0.44	-1.04	-1.10	**CP 30**	0.07	-0.86	-0.45
CP 36	0.19	-0.64	1.04	**CP 33**	-1.32	-0.37	0.81
CP 37	-0.44	0.98	0.84	**CP 34**	0.04	-0.45	0.27

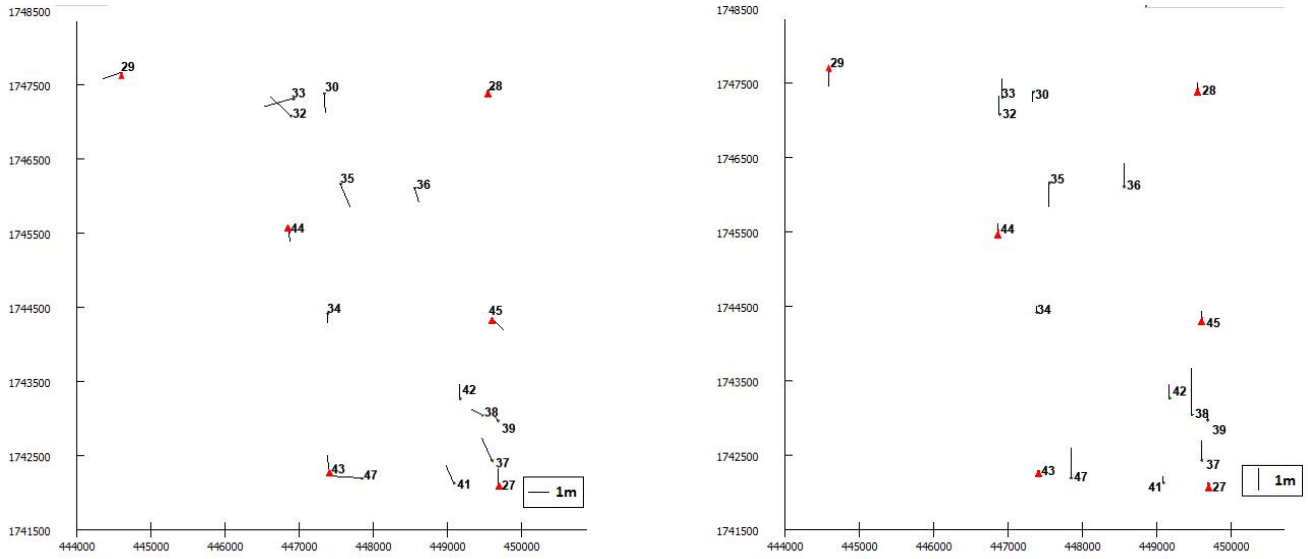

(a) horizontal resultant (b) vertical shift

Figure (11): Horizontal resultant (Right) and vertical shift (Left) for the GCPs and 12 CP of Case 3

At Case 3, the same trend for the horizontal residuals in east and north direction was recorded. However a little bit enhancement was observed for the vertical residuals. From table (6) it can be seen that the absolute shift in east direction ranges from 0.00 m to 1.40 m and the shift in north direction range from 0.05 m to 1.04 m. Accordingly the horizontal resultant ranges from 0.23 m to 1.40 m, where figure (11a) illustrates the horizontal resultant values. The height shift ranges from 0.27 m to 2.05 m that shows at figure (11b).

Table (7): Results of Case 4 (8 GCPs and 12 CPs)

Pnt	RX	RY	RZ	Pnt	RX	RY	RZ
GCP 27	0.15	0.58	-0.20	**CP 39**	0.03	0.10	0.07
GCP 28	0.49	-0.03	0.00	**CP 41**	-0.18	0.68	0.03
GCP 29	-0.61	-0.36	-0.96	**CP 47**	-1.23	0.00	1.11
GCP 43	0.07	0.63	-0.38	**CP 32**	-0.74	0.76	0.58
GCP 44	0.20	-0.54	0.03	**CP 42**	0.16	0.55	0.35
GCP 45	0.94	-0.86	0.03	**CP 30**	0.23	-0.94	-0.70
GCP 46	-0.17	0.28	-0.20	**CP 33**	-1.16	-0.46	0.56
GCP 48	-0.91	0.43	1.67	**CP 34**	0.20	-0.54	0.03
CP 37	-0.27	0.90	0.60	**CP 35**	0.60	-1.13	-1.34
CP 38	-0.30	0.15	1.81	**CP 36**	0.36	-0.73	0.79

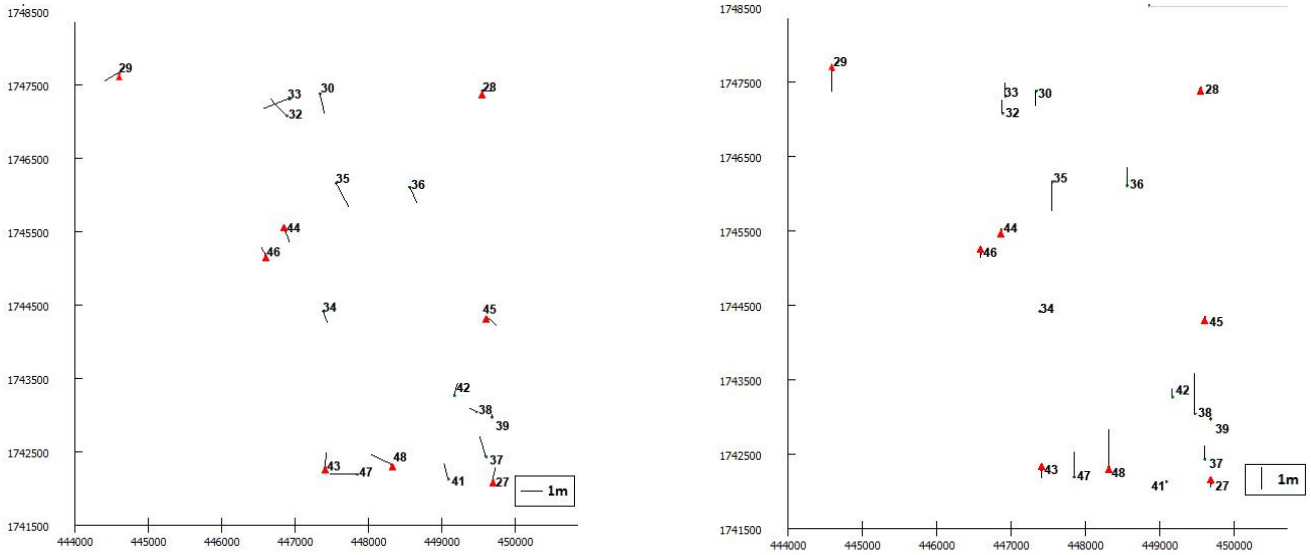

(a) horizontal resultant (b) vertical shift

Figure (12): Horizontal resultant (Right) and vertical shift (Left) for the GCPs and 12 CP of Case 4

A significant enhancement was recorded at case 4, while as presents at table (7), the absolute shift in east direction ranges from 0.03 m to 1.23 m and the absolute shift in north direction ranges from 0.00 m to 1.13 m that yields the horizontal resultant values to be from 0.10m to 1.28m. These horizontal resultant values are illustrated in figure (12a). Similarly, 40% enhancement for height shift was observed as illustrated at figure (12b), where the values range from 0.00 m to 1.81m.

Table (8): Results of Case 5 (10 GCPs and 12 CPs)

Pnt	RX	RY	RZ	Pnt	RX	RY	RZ
GCP 27	0.24	0.63	-0.31	**CP 41**	-0.08	0.72	-0.08
GCP 28	0.58	0.01	-0.11	**CP 47**	-1.14	0.04	0.99
GCP 29	-0.51	-0.31	-1.07	**CP 32**	-0.65	0.80	0.47
GCP 43	0.16	0.67	-0.49	**CP 42**	0.26	0.59	0.24
GCP 44	0.30	-0.49	-0.08	**CP 30**	0.33	-0.90	-0.81
GCP 45	1.04	-0.82	-0.08	**CP 33**	-1.06	-0.41	0.45
GCP 46	-0.07	0.33	-0.31	**CP 34**	0.30	-0.49	-0.08
GCP 48	-0.82	0.47	1.56	**CP 35**	0.70	-1.08	-1.45
GCP 49	-0.58	-0.29	0.09	**CP 36**	0.45	-0.68	0.68
GCP 50	-0.35	-0.21	0.80	**CP 37**	-0.17	0.94	0.48
CP 39	0.12	0.14	-0.04	**CP 38**	-0.20	0.19	1.70

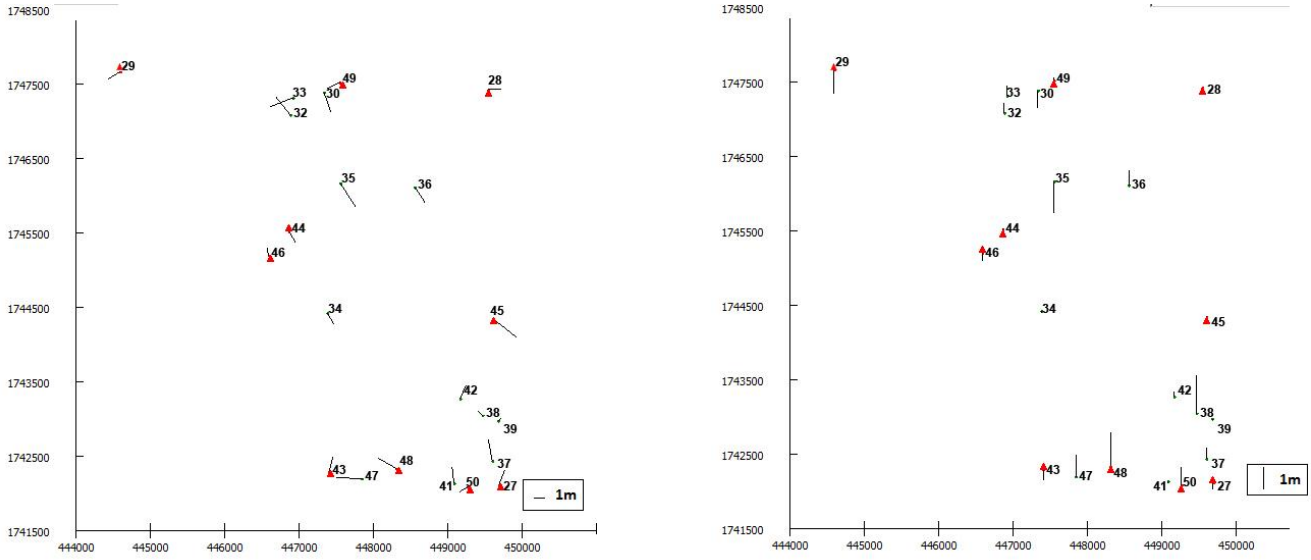

(a) horizontal resultant (b) vertical shift

Figure (13): Horizontal resultant (Right) and vertical shift (Left) for the GCPs and 12 CP of Case 5

As it is in case 4, the absolute shift in east direction ranges from 0.07 m to 1.14 m and the shift in north direction ranges from 0.01 m to 1.08 m. Hence, the horizontal resultant ranges from 0.19 m to 1.32 m as shown in figure (13a). As well as, Figure (13b) illustrates the case of height shift for case 5, where the values range from 0.04 m to 1.17 m.

Meanwhile, the following calculations were prepared to determine the RMS error in easting, northing directions and height respectively.

$$RMSeE = \sqrt{\frac{1}{n}\sum_{i=1}^{n} \Delta Ei^2} \quad (6)$$

$$RMSeN = \sqrt{\frac{1}{n}\sum_{i=1}^{n} \Delta Ni^2} \quad (7)$$

$$RMSeZ = \sqrt{\frac{1}{n}\sum_{i=1}^{n} \Delta Zi^2} \quad (8)$$

RMSeE = Root Mean Square error in E direction
RMSeN = Root Mean Square error in N direction
RMSeZ = Root Mean Square error in Z
ΔEi^2 = the X Residual for GCP ***i***
ΔNi^2 = the Y Residual for GCP ***i***
ΔZi^2 = the Z Residual for GCP ***i***
i = GCP Number
n = the number of GCP

The results indicate that the accuracy of the proposed technique for DEM generation should be tested in order to reach the best accuracy. The root mean square error

(RMSe) between estimations and observations of altitude at the study site are presented in Table (9) and (10). The RMSe ranged between ± 1.05 and ± 0.81 m.

Case one, 3 Ground control points, yielded the worst estimations for topography with RMSE of ± 1.05m. Case two, 4 ground control points, performed almost the same as case one with RMSE of ± 1.05. Case three, 6 ground control points, yielded slightly better estimations for topography with RMSE of ± 0.97m. Case four, 8 ground control points, yielded significant better estimations for topography than case three with RMSE of ± 0.84m. Once again, case five, 10 ground control points, increases the accuracy only slightly with RMSE of ± 0.81m.

Table (9): summarizes the RMSe for GCP per each case

Number of Ground control points	RMSeE	RMSeN	RMSeZ
03 Ground control points	± 0.46	± 0.39	± 0.41
04 Ground control points	± 0.40	± 0.43	± 0.36
06 Ground control points	± 0.47	± 0.55	± 0.35
08 Ground control points	± 0.55	± 0.52	± 0.70
10 Ground control points	± 0.55	± 0.48	± 0.69

Table (10): summarizes the RMSe for12 CPs per each case

Number of Ground control points	RMSeE	RMSeN	RMSeZ
03 Ground control points	± 0.61	± 0.68	± 1.05
04 Ground control points	± 0.62	± 0.68	± 1.05
06 Ground control points	± 0.67	± 0.67	± 0.97
08 Ground control points	± 0.59	± 0.67	± 0.84
10 Ground control points	± 0.58	± 0.67	± 0.81

In this study 10 GCPs were used and about 60 tie points were generated automatically, and the RPC model was corrected by the 3rdorder polynomials. The results indicate that, the RMS of horizontal and vertical residuals at the GCPs and check points were around one pixel. Thus the 3D model from IKONOS stereo imagery is accurate enough for rectifying the IKONOS HRS stereo-pair with the accuracy of the 1:10,000 contour maps.

7.2. Evaluation of the Produced DEM

The resulted DEM was then evaluated through the integration of the high accuracy RTK topographic survey data for about 600 points, which was conducted for the study area. The detailed analyses of the DTM performed through the comparison with the GPS measured points. Results are shown in table (11) and figure (14)

Table (11): Statistics of height differences between DTM and GPS data

Residuals (Height Difference)	Frequency	Percentage %	Residuals (Height Difference)	Frequency	Percentage %
0.00 :-0.25	96	16.4%	0.0 0.25	79	13.5%
-0.25:-0.5	108	18.4%	0.25:0.50	43	7.3%
-0.50 :-0.75	85	14.5%	0.50 :0.75	37	6.3%
-0.75:-1.00	39	6.6%	0.75:1.00	12	2.0%
-1.00 :-1.25	32	5.5%	1.00 : 1.25	6	1.0%
-1.25:-1.50	19	3.2%	1.25:1.50	5	0.9%
-1.50 :-1.75	7	1.2%	1.50 :1.75	5	0.9%
-1.75:-2.00	3	0.5%	1.75:2.00	0	0.0%
-2.00:-2.25	3	0.5%	2.00 :2.25	3	0.5%
-2.25:-2.50	4	0.7%	1.0 0.25	79	13.5%
-2.50 :-2.75	1	0.2%			

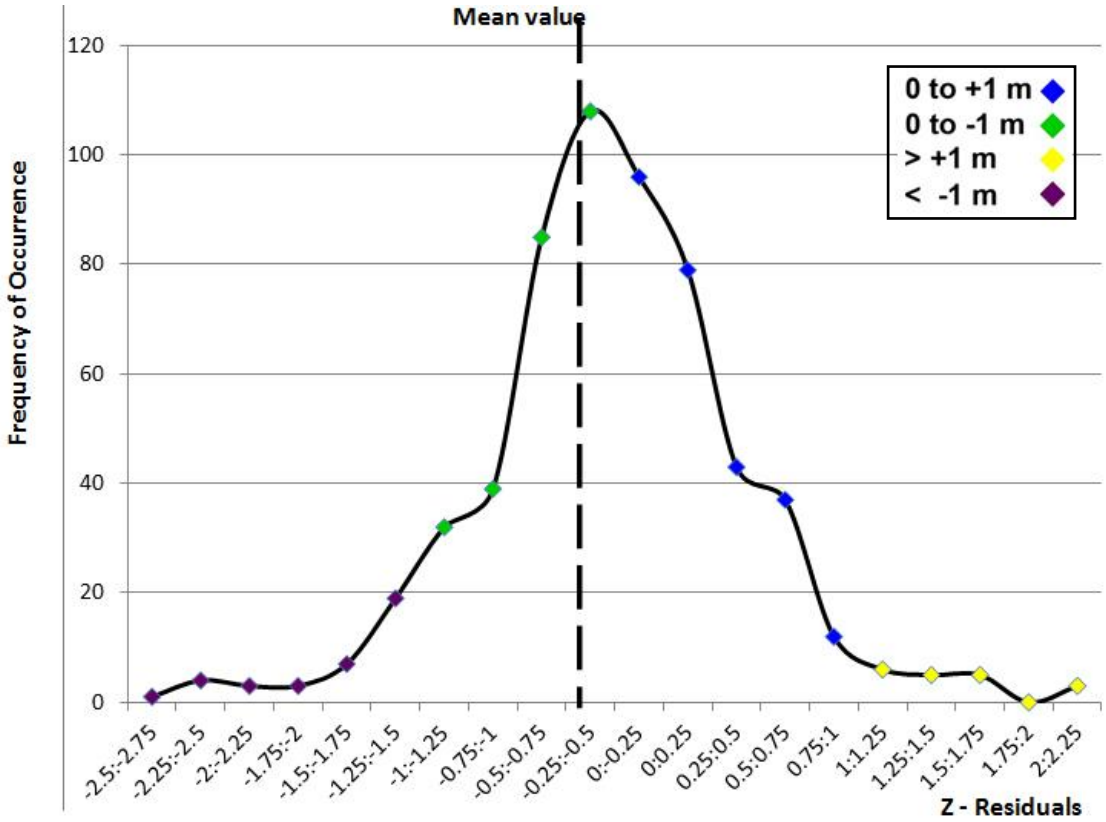

Figure (14): Frequency of occurrence versus Z-residuals

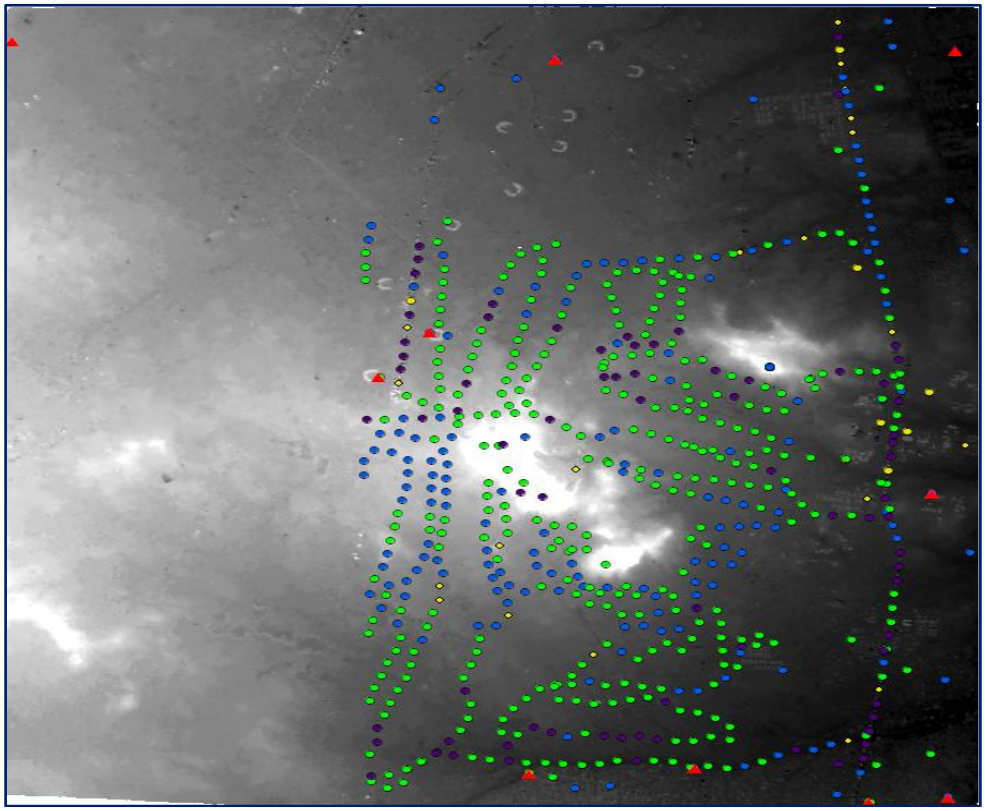

Figure (15): height difference distribution of DEM

The proposed method exhibited few prediction errors over 2m. Surprisingly, a relatively large data scattering (82.5%) is found to be between 0m and ± 1m indicating the low differences between estimations and observations and hence the accurate performance of the method.

One question still remains, why most of the estimated heights are lower than the corresponding observed heights. One possible reason for that can be the method of image acquisition in case of IKONOS stereo pair, an image collected at a low elevation angle (above 60 degrees) as well as an image collected at a higher elevation angle (above 72 degrees) with 30°- 45° convergence (0.54 to 0.83 base-to-height ratio) as previously mentioned.

8. CONCLUSIONS

In this research, an attempt is made to develop a workflow for DTM production using IKONOS HRS stereo-pair. The workflow comprises all necessary technical steps of dealing with satellite imagery until extracting desired image information. An experimental test DTM generation is investigated. Based on the test results, the following concluding remarks can be made:

- Table (11) shows that almost the 83% of the points are within ±1m.
- From figure (14) and figure (15), the automated DTM extraction process commonly has some difficulties in urban areas specifically around buildings, bridges, trees, and other extruding features on the earth's surface.

- The accuracy of the sensor model and the high correlation of the image matching Parameters and the software used for autocorrelation measurement of height-points are the three principal factors of getting the expected DEM accuracy.
- The research compared the heights at each point where the horizontal coordinates of two DEMs are the same. The average vertical difference (absolute values) of 605 points was0.65m while the Root Mean Square Error (RMSE) was 1.01. Thus the produced 3D model from IKONOS stereo imagery is accurate enough to meet the accuracy of the 1:10,000 contour maps.
- In general, the RMSE value should be within two times of the original pixel size of the imagery for the output DTM to be considered accurate to real-world conditions.
- Topography roughness has much significant negative impact on the quality of DEMs generated from HRS elevation data as shown in figure14 and figure15.
- Available GPS and IKONOS HRS stereo-pair were sufficient for rectifying the IKONOS image with the accuracy of the 1:10,000 contour maps.

FURTHER WORK

- The extracted elevation data from High Resolution Stereo-Optical satellite Imagery will be used with different mathematical models to refine and improve the solution for different areas.
- Using Extracted Digital elevation model for Accuracy Assessment of Ortho-rectification of high resolution satellite image.
- Evaluation of Feature Extraction from anaglyph, and check the optimum contour interval for extracted contour maps from produced digital elevation model.

REFERENCES

- Chen, L. C. and Lee, L. H., (1993): "Rigorous Generation of Digital Orthophotos from SPOT Images". Photogrammetric Engineering and Remote Sensing, 59(3):655–661.
- ELASHMAWY, N., ELMANADILI, Y., and BARAKAT, H., (2005): "Comparative Analysis and Evaluation of Various Mathematical Models for Stereo IKONOS Satellite Images". FIG Working Week 2005. Available at: https://fig.net/pub/cairo/papers/ts_27/ts27_03_elashmawy_etal.pdf. Last accessed at 19 July 2012.
- Fraser, C.S., Hanley, H.B. and Yamakawa, T. (2002): "Three-dimensional positioning accuracy of Ikonos imagery". The Photogrammetric Record, VOL.17, NO.99, 465-479.
- Gar Alnabi, I., Elshami and Awadelgeed, M., (2011b): "Accuracy Assessment Of SRTM Elevation Data". Sudan Engineering Society Journal, March 2011, Volume 57; No.l.
- Gar Alnabi, I., Elshami, M., Awadelgeed, M., (2011a): "Quality Assessment of DEMs Derived from 1:100,000 Scale Topographic Maps". UofKEJ Vol. 1 Issue 1 pp. 32-40 (June 2011). Available online at ejournals.uofk.edu.
- Hu, Y., Tao, V., and Croitoru, A., (2004): "Understanding the Rational Function Model: Methods and Applications". The International Archives of Photogrammetry and Remote Sensing, Istanbul, Turkey.

- Iida, Y., Matsuo, K. and Sato, J. (2001): "A Study of Making1:25,000 Topographic Maps by Using High-resolution Satellite imagery". Proceedings of Regular Conference of Japan Cartographers Association.
- LeromeKoronaa, Etienne Berthier B. C., .Marc Bernard A., Frederique Rernyb, c., and Eric Thouven, (2009): "SPIRIT SPOT5 Stereoscopic Survey of Polar Ice: Reference Images and Topographies During the Fourth International Polar rear (2007_2009)". ISPRS Journal of Photogrammetry and Remote Sensing .Vol l)-I. pp 20-i_212.
- McGlone, C., (1996): "Sensor Modeling in Image Registration". Digital Photogrammetry, An Addendum to the Manual of Photogrammetry, Chapter 5, American Society for Photogrammetry and Remote Sensing.
- Poli, D... Zhang, L., and Gruen. A., (2004): "SPOTS-HRS Stereo Images Orientation and Automated DSM Creation". IAPRS Vol 35, Istanbul.
- Satellite Imaging Corporation, (2012): "IKONOS Stereo Satellite Imagery". Available at: http://www.satimagingcorp.com/svc/ikonos-stereo-satellite-images.html. Last accessed at 19 July 2012.
- Tao, C., Hu, Y., Mercer, J., Schnick, S. and Zhang, Y., (2000): "Image Rectification Using a Generic Sensor Model- Rational Function Model". The International Archives of Photogrammetry and Remote Sensing, Vol. 33, Part B3, pp. 874-881, Amsterdam, The Netherlands.
- Tao, C., Hu, Y., (2001): "A comprehensive study on the rational function model for photogrammetric processing".PE&RS, 67(12), pp. 1347-1357.
- Thomas, R., (2002): "Digital Map Updating from Satellite Imagery", IAPRS, Volume XXXIV, Part2, Commission II, Xi'an, Aug.20-23, 2002.
- Toutin. T., (2001): "DEM Creation from New VIR Sensors: IKONOS, ASTER and lansat-7", In PROCEEDINGS, IEEE-IGARSS, Sydney, Australia.
- WANG Xue-junl , FU Xiao2, XU Mao-song l, (2008): "Effect of Incidence Angle and Accuracy of DEM on Quality of SPOTS Ortho-image Map", Chineese Journal. 2008 (SI), pp 134-137.
- Zhen, X., Huang, X., and K woh, L., K., (2001): "Extracting DEM from SPOT Stereo Images", 20 Asian Conference on Remote Sensing, Singaphore.